ACS OMEGA

http://pubs.acs.org/journal/acsodf

Article

Low-Dose Element-Doped CeCrM/TiO_2 (M = La, Cu, Fe, LaCu, LaFe) Catalyst for Low-Temperature NH_3-SCR Process: Synergistic Effect of LaCu/LaFe

Guilin Mu, Shuai Liu, Qingjie Liu, Shanshan Liu,* and Xintang Zhang*

Cite This: *ACS Omega* 2022, 7, 37694−37704

Read Online

ACCESS | Metrics & More | Article Recommendations

ABSTRACT: A series of CeCrM/TiO_2 (M = La, Cu, Fe, LaCu, LaFe) catalysts were prepared via impregnation method and are employed as low-temperature NH_3-SCR catalysts. The present study investigates the low-dose element doping on the TiO_2-supported catalyst to improve the NH_3-SCR performance. And CeCrLaCu/TiO_2 exhibited the best catalytic performance (NO conversion approaching 100% at 260−420 °C). The characterization results show that the synergistic effect of LaCu and LaFe on the catalytic performance was more obvious than that of Cu, Fe, and La alone. The doping of LaCu/LaFe decreased the specific surface area of the catalyst but increased the dispersion, surface acidity, and reducibility of the catalyst. Moreover, LaCu/LaFe promoted the formation of valence state distribution and oxygen vacancy content on the surface of the catalyst. There were more Ce^{3+}, Cr^{6+}, Cu^{+}, and oxygen adsorbed on the surface of the CeCrLaCu/TiO_2 catalyst. H_2-TPR analysis showed that the synergistic effect of LaCu was more likely to promote the reduction of Cr and Cu and increase the reduction degree of metal oxides. However, Fe is easier to coordinate with La, thus improving the redox performance of the catalyst. Compared with CeCrLaFe/TiO_2, the ammonia adsorption capacity of CeCrLaCu/TiO_2 is better. Therefore, the synergistic effect of LaCu can promote the reaction performance of NH_3-SCR better.

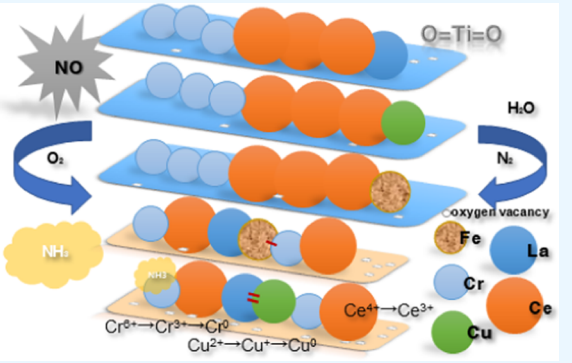

1. INTRODUCTION

Nitrogen oxides (NO_x) derived from the burning of fossil fuels such as coal, oil, etc., are harmful to human beings and the environment. As one of the main polluting gases, NO_x not only causes acid rain and photochemical pollution but is also a major component of PM 2.5.[1] Thus, it is imperative to control the emission of harmful NO_x. In recent years, selective catalytic reduction of ammonia (NH_3-SCR) has been widely used in NO_x removal. In this process, NH_3 acts as a reducing agent to reduce NO_x to harmless N_2 and H_2O with the action of the catalyst, which is the core of NH_3-SCR technology. At present, the commercial catalyst for NH_3-SCR is mainly a V_2O_5-based catalyst, which shows excellent catalytic performance in the NH_3-SCR reaction in the temperature range of 300−400 °C. However, the catalyst has disadvantages, such as narrow operating temperature window, toxicity of VO_x species, inactivation of alkali metals, and decrease of N_2 selectivity at high temperatures.[2] Therefore, non-V_2O_5-based catalysts have been extensively studied.

Currently, anatase TiO_2, Al_2O_3, molecular sieves, and carbon-based materials are usually used as denitrification catalyst supports. The supports are important for the SCR reaction. A good support can disperse the active components well. Moreover, the interaction of supports and active components also has an important effect on the catalytic performance.[3] Therefore, anatase TiO_2 has been widely studied due to its low cost, good sulfur resistance, nontoxicity,[4] and rich Lewis acid sites.[5]

In addition, catalysts with polymetallic oxides as active components can improve the NH_3-SCR performance due to the synergistic effect between components, which has also been widely studied.[6−8] Ce-based catalysts are expected to be potential substitutes for V_2O_5-based catalysts. CeO_2 is widely used as NH_3-SCR catalysts for excellent redox ability of Ce^{4+}/Ce^{3+} reversible redox pair, abundant surface oxygen vacancy, and high oxygen storage capacity.[9−13] The oxidation state of chromium oxide (CrO_x) is variable, especially for exposed chromium ions, and the most common valence states are Cr^{3+} and Cr^{5+}.[14] The presence of Cr makes the surface acidity and reducibility of the CeZr catalyst stronger, and more ad-NO_x and ad-NH_3 on the catalyst surface are conducive to the NH_3-SCR

Received: July 21, 2022
Accepted: October 4, 2022
Published: October 12, 2022

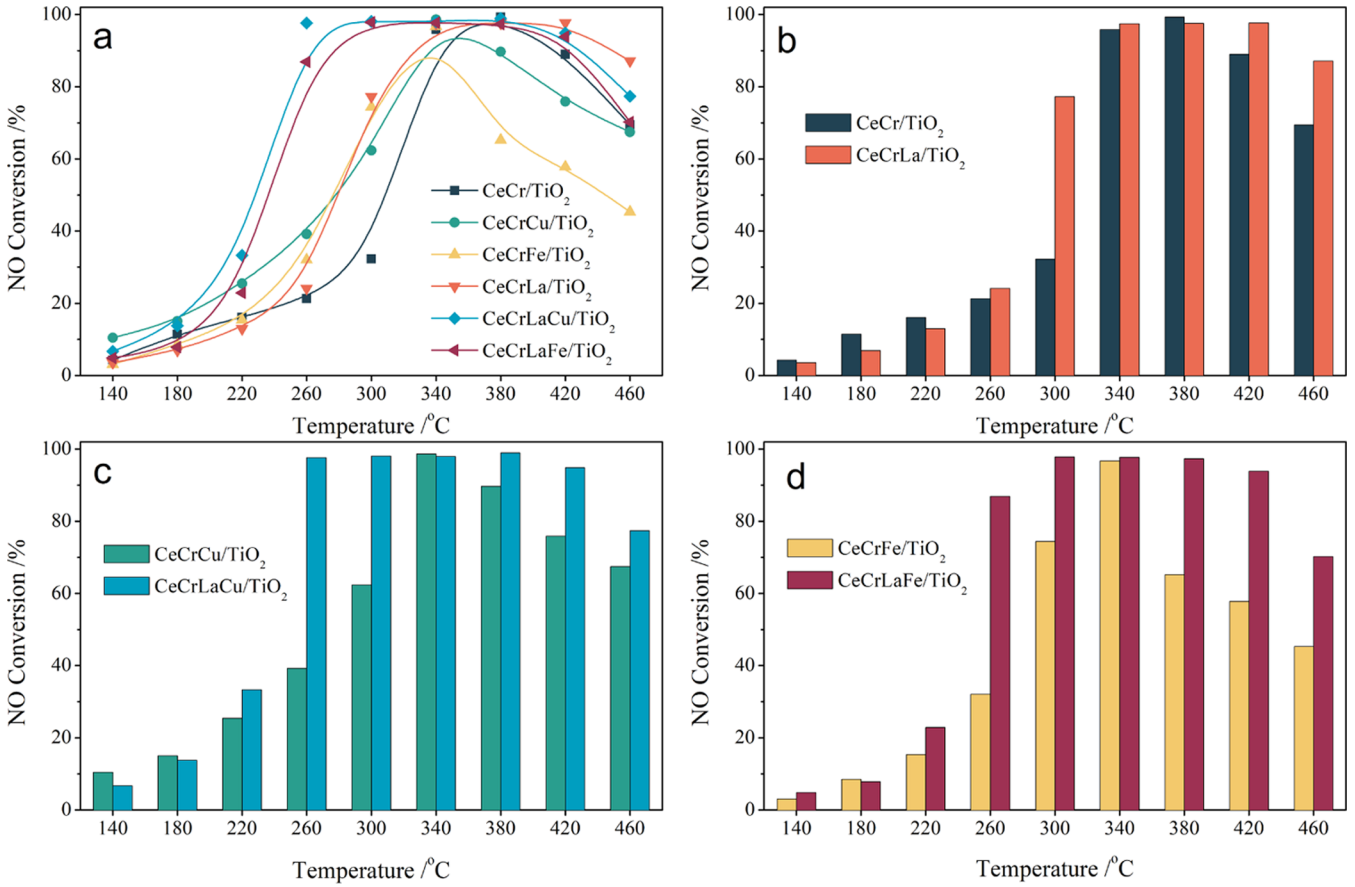

Figure 1. NO conversion of (a) all catalysts, (b) $CeCr/TiO_2$ and $CeCrLa/TiO_2$ catalysts, (c) $CeCrCu/TiO_2$ and $CeCrLaCu/TiO_2$ catalysts, and (d) $CeCrFe/TiO_2$ and $CeCrLaFe/TiO_2$ catalysts. Reaction conditions: [NO] = [NH_3] = 1000 ppm, [O_2] = 5%, N_2 balance, GHSV = 20,000 h^{-1}.

reaction.[15−17] Furthermore, Ce can promote the conversion between Cr^{3+} and Cr^{6+} and increase the proportion of lattice oxygen, which improves the activity of the catalyst.[18] Thus, the interaction between Ce and Cr can improve the redox property and accelerate the redox circle, which are beneficial to the improvement of NH_3-SCR activity.

However, the mass percentages of Cr and Ce in most of the catalysts prepared by researchers are greater than 5%,[19] and some even exceed 30%.[20] The low-dose CeCr/Ti catalyst has limited redox performance and acidity, which is insufficient to show excellent NH_3-SCR activity. To optimize the catalytic performance, the supported catalyst can be doped with some transition metals to improve the catalytic activity through the synergistic effect of multiple metals.[21] Due to the synergistic effect between metals, the bimetallic electron transport cycle serves as a bridge to accelerate the electron transfer from NO molecules to O_2 molecules, promoting the generation of NO_2 and accelerating the fast-SCR.[22] Lanthanide is a rare earth element abundant in China. La-doped catalysts have been widely studied in SCR reactions due to their excellent oxygen storage capacity and unique redox properties.[23,24] Studies have shown that La^{3+} could be partly integrated into ceria fluorite lattice to induce an expansion of the crystal cell dimensions, which concomitantly induces more lattice defects and improves the lattice oxygen mobility.[25] Yi et al.[26] studied the effects of rare earth element (La, Ce) modification on oxidation performance, and the results showed that La, Ce modification could promote the oxidation performance of adsorbents and reduce the pore diameter of the adsorbents. Therefore, the interaction between Ce and La is also conducive to the improvement of NH_3-SCR activity.[27]

The state of Cu species has a great impact on the SCR activity of the CeO_2−CuO catalyst,[28] and Cu^{2+} can improve the low-temperature activity, while CuO would decrease the high-temperature activity. The interaction between Cu and Ce can reduce the crystallinity of CeO_2, enhance the oxygen storage capacity and acidity of the catalyst, and increase the types of Ce^{3+} species.[29] Thus, the interaction between Cu and Ce is helpful to improve the surface acidity and redox performance of the catalyst. In addition to copper, the presence of Fe can increase the surface area, enhance the redox properties, increase the number of surface acid sites, and increase the surface adsorbed oxygen.[30] Zhang et al.[31] reported that Fe^{3+} replaces Ce^{4+} to form Ce−Fe solid solution. This change of crystal phase structure facilitated the homogeneous dispersion of the active component on the catalyst surface, increased acid sites and specific surface area, and exposed more oxygen vacancies. Ge et al.[32] found that the addition of Cr greatly increased the specific surface area, the number of weak and medium-strong acid sites, and the ratio of Fe^{3+}/Fe^{2+} on the surface of the Fe/AC catalyst, thus promoting the low-temperature SCR activity of the catalyst. Therefore, the interaction between Fe and Ce or Cr helps to improve the redox capacity and the number of acid sites on the catalyst.

The composition of coal-fired flue gas in China is complex, often containing components such as SO_2 and H_2O, which will seriously damage the activity and stability of the NH_3-SCR catalyst. Furthermore, the deactivation of the low-temperature $DeNO_x$ catalyst was more severe when SO_2 and H_2O were

https://doi.org/10.1021/acsomega.2c04603
ACS Omega 2022, 7, 37694−37704

present at the same time, suggesting that SO_2 and H_2O appeared to exhibit synergistic toxicity in catalyst poisoning.[33] For example, the metal element Cu easily reacts with sulfuric acid generated by H_2O and SO_2, resulting in the lack of active components and additives, and the sulfate species generated on the surface of the catalyst consumes the active Cu^{2+} species and occupies the main active sites, thereby reducing nitric acid. The types of salt species and intermediates lead to bad NH_3-SCR activity.[34] In this study, it can be known from XPS that after adding La ($CeCrLaCu/TiO_2$), Cu^{2+} decreases and Cu+ increases, so it can reduce the formation of sulfate with sulfuric acid, thereby inhibiting poisoning. Hao et al. concluded with the XPS results that part of Fe^{2+} was oxidized to Fe^{3+} during the reaction, and the Fe^{2+} species had strong redox ability, which could explain the reason for the decrease in activity after the reaction. In addition, SO_2 and H_2O induce Ce transformation from Ce^{4+} to Ce^{3+} on the catalyst surface, which increases the amount of chemisorbed oxygen. Due to these factors, the addition of Ce and Fe species contributes to the excellent tolerance of the catalyst to SO_2 and H_2O.[35] According to the change of Ce ion content in XPS in this paper, the Ce^{3+} content in $CeCrLaCu/TiO_2$ is the highest (58%), which increases the content of chemisorbed oxygen as described in the literature, thereby improving the water resistance and sulfur resistance of the $CeCrLaCu/TiO_2$ catalyst. Denitration catalyst poisoning is one of the key problems leading to substandard emission in flue gas during the denitration process. It is of great significance to improve the catalytic performance of SCR denitration catalysts, reduce the use cost of denitration catalysts, and avoid its poisoning.

Hydrothermal stability refers to the property of catalytic cracking catalysts in industrial application. At high temperatures and in the presence of water vapor, the structure is not damaged and has the ability to maintain sufficient equilibrium activity. However, hydrothermal aging usually occurs on molecular sieve catalysts. Under high-temperature hydrothermal aging conditions of 650 °C and above, the structure of molecular sieves, the properties of active species, and other physical and chemical properties will still undergo significant changes, which may cause irreversible loss of catalysts.[36] There are also few studies on the hydrothermal stability of composite metal oxides. In this paper, the hydrothermal stability of the catalyst was also investigated by the NO conversion rate after hydrothermal aging.

In this paper, the low-dosed $CeCrM_x/TiO_2$ (M = La, Cu, Fe, LaCu, LaFe) catalyst was prepared by an impregnation method, and its low-temperature NH_3-SCR performance was investigated. The promotion of metal doping on NH_3-SCR over the $Ce_{0.004}Cr_{0.003}M_x/TiO_2$ catalyst was studied by N_2 physical adsorption (BET), X-ray diffraction (XRD), scanning electron microscopy (SEM), X-ray photoelectron spectroscopy (XPS), temperature-programmed reduction by hydrogen (H_2-TPR), and temperature-programmed desorption by NH_3 (NH_3-TPD). The effects of different metal doping on the redox performance and NH_3 adsorption performance of the catalyst were discussed, and the optimum ratio was selected. The synergistic effect of bimetallic elements of the LaCu/Fe metal-doped catalyst on catalytic activity was also elucidated.

2. RESULTS AND DISCUSSION

2.1. Performances of NH_3-SCR. NH_3-SCR performance of $CeCr/TiO_2$, $CeCrCu/TiO_2$, $CeCrFe/TiO_2$, $CeCrLa/TiO_2$, $CeCrLaCu/TiO_2$, and $CeCrLaFe/TiO_2$ catalysts was evaluated, and the results are illustrated in Figure 1. With the increase of temperature, the NO conversion of the catalysts increases, and $CeCrM/TiO_2$ (M = La, Cu, Fe) reaches the maximum NO conversion (98.9%) at 340 °C. Then, the NO conversion of the $CeCrM/TiO_2$ (M = Cu, Fe) catalyst decreases rapidly, while the NO conversion of the $CeCrLa/TiO_2$ catalyst remains stable in the temperature range of 340−420 °C. Compared with $CeCrFe/TiO_2$ catalysts, $CeCrLa/TiO_2$ catalysts have better high-temperature activity and a wider operating temperature window, which indicates that the addition of La is more favorable for the high-temperature activity (as shown in Figure 1a). And the addition of Cu, compared with Fe and La, produced a limited improvement in the low-temperature activity of the catalyst in the temperature range of 140−260 °C. However, the modification effects of La, Fe, and Cu are limited.

To further improve the low-temperature activity of the catalyst, considering the excellent redox performance of Cu and Fe, the CeCr/Ti catalyst was doped with LaCu and LaFe, respectively. As shown in Figure 1c, the NO conversion curve of $CeCrLaCu/TiO_2$ is shifted toward lower temperature by 80 °C compared to $CeCrLa/TiO_2$ (Figure 1b). In addition, 100% NO conversion is maintained until 420 °C, the temperature at which the conversion starts to decrease. The $CeCrLaFe/TiO_2$ catalyst (Figure 1d) reaches the maximum NO conversion (99%) at 300 °C. When the temperature exceeds 380 °C, the NO conversion drops rapidly to reach 70% at 460 °C. Consequently, the $CeCrLaCu/TiO_2$ and $CeCrLaFe/TiO_2$ catalysts effectively broadened the NO conversion at low temperatures. This indicates that the introduction of La can greatly improve the low-temperature catalytic activity of catalysts (Figure 1b−d), especially in the catalysts containing Cu and Fe. In addition, it was found that the interaction between La and Cu was more conducive to NH_3-SCR performance at low temperatures.

2.2. Physicochemical Properties. *2.2.1. XRD Analysis.* The XRD patterns of the catalysts are shown in Figure 2. All

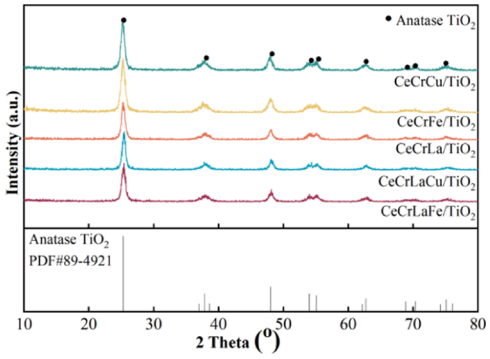

Figure 2. XRD patterns of all samples.

samples display diffraction peaks at 25.3, 37.8, 48.1, 53.9, 55.1, 62.8, 68.7, 70.4, and 75.1°, which correspond to anatase TiO_2 phase peaks [PDF-JCPDS 89-4921]. No independent diffraction peaks related to CeO_x, CrO_x, LaO_x, CuO_x, and FeO_x were observed in samples. This indicates that the active components are in a highly dispersed state or the amount of active component is below the detection threshold. The good dispersion facilitated good contact of the active components with each other and led to strong interactions between Ti and other metal oxides.[37] Compared with the diffraction peaks of $CeCrFe/TiO_2$, $CeCrCu/TiO_2$, and $CeCrLa/TiO_2$ catalysts, the weakened diffraction peak intensities of $CeCrLaCu/TiO_2$ and $CeCrLaFe/TiO_2$ catalysts indicate that the interaction of La and

https://doi.org/10.1021/acsomega.2c04603
ACS Omega 2022, 7, 37694−37704

Cu/Fe reduces the crystallinity of the catalysts, which is in agreement with the previous report.[38] According to the Debye–Scherrer's formula, the crystalline size is calculated and listed in Table 1. The crystal size increased in the following sequence:

Table 1. XRD and BET Results of All of the Samples

samples	crystal size[a] (nm)	BET surface area (m^2/g)	pore volume (cm^3/g)	average pore diameter (nm)
$CeCrCu/TiO_2$	9.1	84.2	0.24	11.1
$CeCrFe/TiO_2$	9.0	117.8	0.28	10.1
$CeCrLa/TiO_2$	8.2	81.8	0.20	9.1
$CeCrLaCu/TiO_2$	8.6	77.1	0.19	9.7
$CeCrLaFe/TiO_2$	8.4	85.0	0.20	9.1

[a]Calculated by Debye–Scherrer.

$CeCrLa/TiO_2$ <$CeCrLaFe/TiO_2$ <$CeCrLaCu/TiO_2$ <$CeCrFe/TiO_2$ <$CeCrCu/TiO_2$. The particle size of the catalyst doped with La is smaller than that without La, indicating that La doping inhibited the crystalline growth of anatase TiO_2.[9] The $CeCrCu/TiO_2$ and $CeCrFe/TiO_2$ catalysts with lower NO conversion had larger crystallite size, while the $CeCrLaCu/TiO_2$ catalyst with the highest NO conversion had smaller crystallite size. The results show that the small crystallite size can promote the NO conversion of the catalyst, but it does not always increase with decreasing crystallite size.

2.2.2. N_2 Adsorption–Desorption Behavior. The N_2 adsorption–desorption isotherms of the catalysts are presented in Figure 3. As shown in Figure 3a, the samples showed isotherms of type III, which exhibited hysteresis loops mostly of type H3, indicating that these samples contained mesopores (2–50 nm). The specific surface area, pore volume, and pore size of all samples are summarized in Table 1. A larger surface area and smaller average pore size contribute to the higher physisorption ability of the catalyst.[39] Compared with $CeCrCu/TiO_2$ and $CeCrFe/TiO_2$ catalysts, the $CeCrLa/TiO_2$ catalyst has a smaller specific surface area and average pore size, but the $CeCrLa/TiO_2$ catalyst has better NO conversion. The addition of composite metal oxides has little effect on the pore volume but has a greater effect on the specific surface area and average pore size. Compared with $CeCrLa/TiO_2$, the addition of the LaCu composite metal oxide leads to a decrease in the specific surface area of the catalyst, while the LaFe composite metal oxide increases the specific surface area of the catalyst. Furthermore, the $CeCrLaCu/TiO_2$ catalyst with the best catalytic activity has the smallest specific surface area and pore volume, indicating that the specific surface area is not the key factor limiting the catalytic activity.

2.2.3. SEM Analysis. SEM test was carried out to observe the morphology of all samples. It can be observed in Figure 4 that there is no significant difference in the morphology of the five catalysts. The catalysts are in the form of particles and they are aggregated. However, the surface of the $CuCeCrLa/TiO_2$ catalyst is relatively smooth compared to other catalysts. The results show that the addition of an appropriate amount of La and Cu improved the dispersity of the active components and reduced the agglomeration.

2.2.4. XPS Analysis. The O 1s, Ti 2p, Ce 3d, Cr 2p, Cu 2p, and Fe 2p photoelectrom profiles of all samples are shown in Figure 5, and their relative atomic concentrations are listed in Table 2.

The O 1s XPS spectra of all catalysts are shown in Figure 5A. The spectra of O 1s could be spilt into two peaks: lattice oxygen (BE = 530.0–530.4 eV, denoted as O_β) and chemisorbed oxygen (BE = 531.6–532.2 eV, denoted as O_α).[40,41] The content of surface adsorbed oxygen over these catalysts is calculated as $O_\alpha/(O_\alpha+O_\beta)$ and listed in Table 2. The mobility of the surface chemisorbed oxygen is stronger than the lattice oxygen; thus, it is easier to participate in the NH_3-SCR reaction.[42−44] In general, the high O_α/O_β relative concentration ratio on the catalyst surface could be related to excellent SCR activity.[45] However, it is obvious from Table 2 that there is a slight difference in O_α over catalysts. The chemical adsorption oxygen species on the $CeCrLaCu/TiO_2$ surface were the most, indicating that the doping of LaCu was more conducive to the generation of chemical adsorption oxygen sites on the catalyst surface. As shown in Figure 5A, according to (c, d, e), the peaks of O_α and O_β over $CeCrLaCu/TiO_2$ and $CeCrLaFe/TiO_2$ catalysts shifted to lower binding energy compared to the $CeCrLa/TiO_2$ catalyst, suggesting the strong interaction among La and Cu/Fe. According to (b, c, e), the peaks of O_α and O_β over $CeCrLaFe/TiO_2$ catalysts shifted to lower binding energy compared to $CeCrLa/TiO_2$ and $CeCrFe/TiO_2$ catalysts, indicating that there is some kind of synergy between La and Fe. According to (a, c, d), the peaks of O_α and O_β over $CeCrLaCu/TiO_2$ catalysts shifted to lower binding energy compared to $CeCrLa/TiO_2$ and $CeCrCu/TiO_2$ catalysts, indicating that there is a certain kind of synergy between La and Fe. This is consistent with previous studies.[46]

XPS of Ti 2p can be fitted into two peaks (Figure 5B). The peaks located at around 458.9 and 464.7 eV could be the result of the orbitals of Ti $2p_{3/2}$ and Ti $2p_{1/2}$, respectively. This indicated

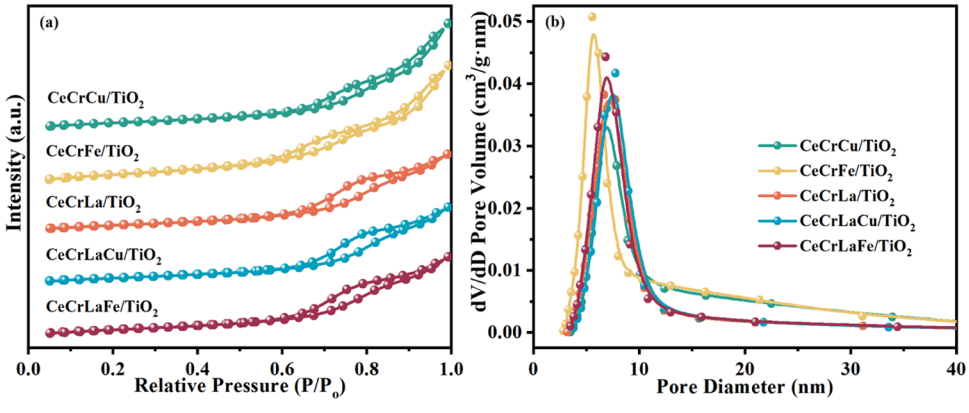

Figure 3. (a) Nitrogen adsorption–desorption isotherms and (b) pore size distributions of the samples.

https://doi.org/10.1021/acsomega.2c04603
ACS Omega 2022, 7, 37694–37704

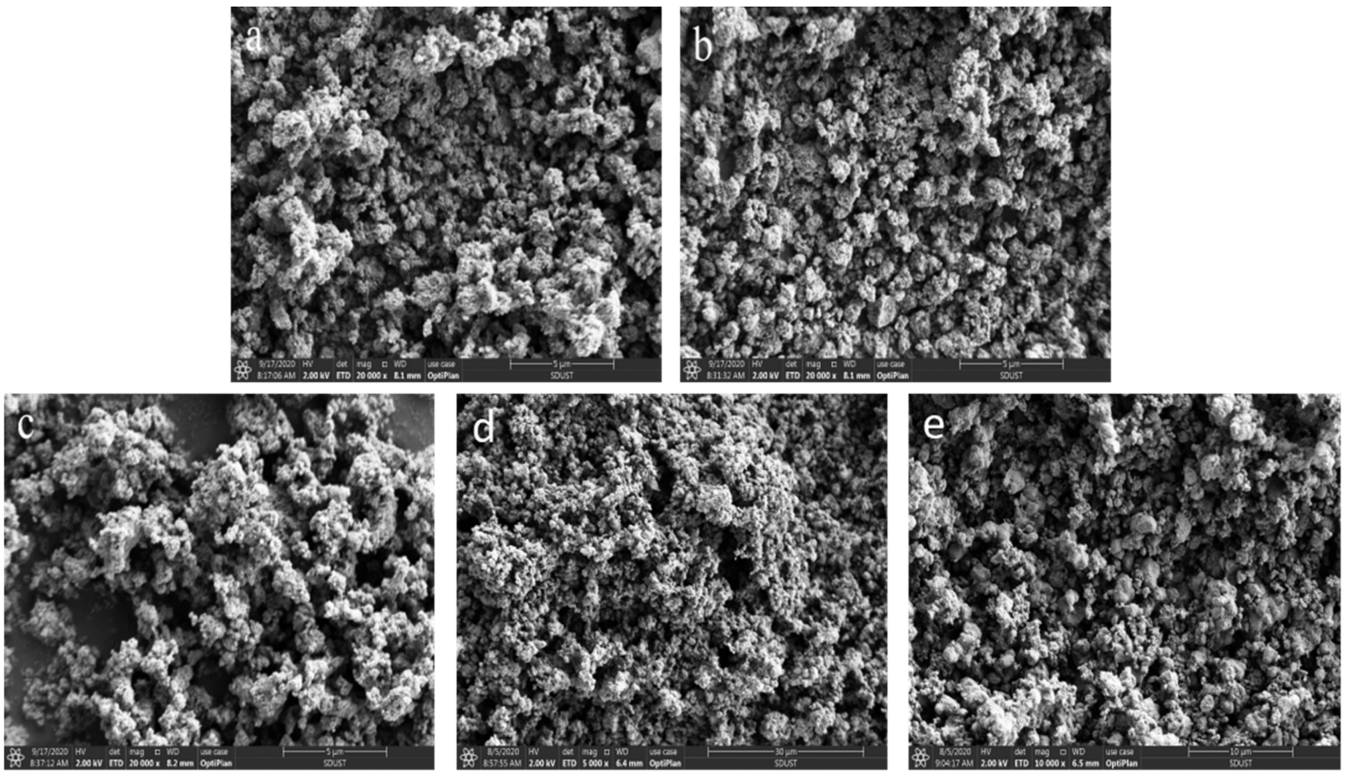

Figure 4. SEM images obtained for (a) CeCrCu/TiO_2, (b) CeCrFe/TiO_2, (c) CeCrLa/TiO_2, (d) CeCrLaCu/TiO_2, and (e) CeCrLaFe/TiO_2.

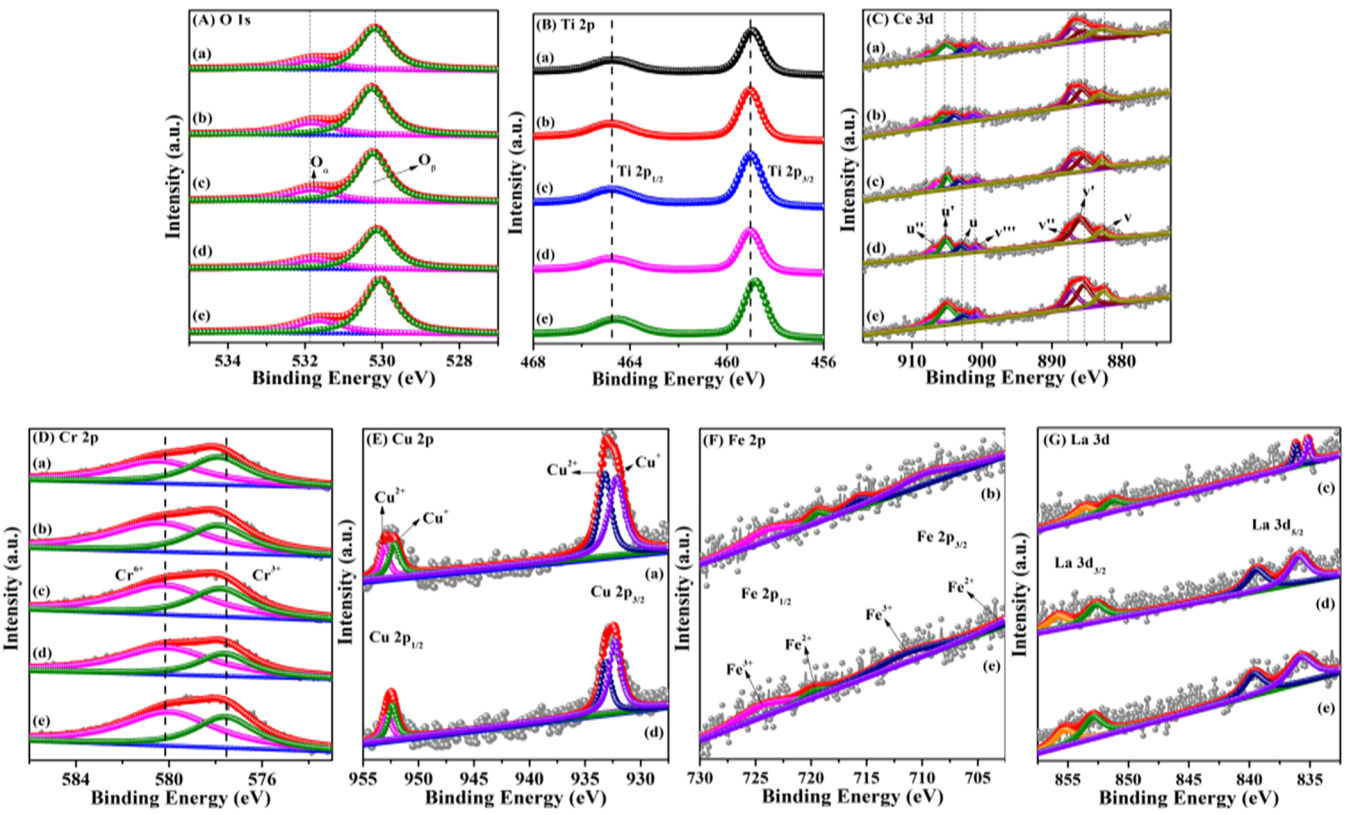

Figure 5. (A) O 1s, (B) Ti 2p, (C) Ce 3d, (D) Cr 2p, (E) Cu 2p, (F) Fe 2p, and (G) La 3d XPS spectra of the samples (a) CeCrCu/TiO_2, (b) CeCrFe/TiO_2, (c) CeCrLa/TiO_2, (d) CeCrLaCu/TiO_2, and (e) CeCrLaFe/TiO_2.

that Ti existed in the Ti^{4+} oxidation state.[47,48] Compared to other catalysts, the Ti 2p peak position of the CeCrLaFe/TiO_2 catalyst was shifted to the right by approximately 0.2 eV, indicating that some of the Ti^{4+} ions were reduced to Ti^{3+} ions. The redox cycle of Ti^{4+}/Ti^{3}+ is hypothesized to be another reason for the high SCR performance.[49]

https://doi.org/10.1021/acsomega.2c04603
ACS Omega 2022, 7, 37694−37704

Table 2. Surface Composition Contents and Redox Properties for the Different Catalysts

samples	surface atomic content[a] (%)						percent of valence state[b] (%)					total H_2 consumption[c] (10^{-5} mmol/g)	H_2 consumption[d] (10^{-5} mmol/g)				
	Ce	Cr	La	Cu	Fe	O	Ti	Ce^{3+}/Ce	Cr^{6+}/Cr	Cu^+/Cu	Fe^{2+}/Fe	O_α/O		I	II	III	IV	V
CeCrCu/TiO_2	0.2	1.5		0.3		59.6	38.4	35	54	55		25	33.4	1.8	3.6	10.2	9.3	8.5
CeCrFe/TiO_2	0.2	1.6			0.3	59.9	38.1	43	63		55	27	33.3	2.5	9.3	10.0	11.5	
CeCrLa/TiO_2	0.2	1.6	0.1			60.5	37.8	44	61			27	23.2	2.5	3.3	7.6	9.8	
CeCrLaCu/TiO_2	0.2	1.5	0.1	0.3		59.6	38.4	58	68	61		28	46.9	3.9	9.8	11.4	9.7	12.1
CeCrLaFe/TiO_2	0.2	1.6	0.1		0.3	60.1	37.8	46	63		23	26	34.3	2.6	2.5	6.2	10.7	12.3

[a]The H_2 consumption over catalysts. [b]The total H_2 consumption over catalysts. [c]The content of various elements determined by XPS. [d]The percent of valence state on the surface of catalysts.

The Ce 3d XPS spectra of the catalysts are presented in Figure 5C. The Ce 3d bands are deconvoluted by the curve-fitting procedure,[9,48,50] and the Ce 3d XPS spectra could be separated into seven peaks and "u" and "v" were attributed to Ce $3d_{3/2}$ and Ce $3d_{5/2}$, respectively. The two peaks labeled u′ and v′ could be assigned to Ce^{3+}, with the remaining peaks of u, u″, v, v″, and v‴ belonging to Ce^{4+}.[51] It is generally believed that Ce^{3+} is related to the appearance of oxygen vacancies. One electron lost by Ce^{4+} combines with O_2 to form O^{2-} (eq 1), which oxidizes NO to NO_2 (eq 2). Therefore, the more Ce^{3+}, the more NO_2 is produced, providing the possibility of a low-temperature L−H mechanism.

$$Ce^{3+} + O_2 + \rightarrow Ce^{4+} + O^{2-} \quad (1)$$

$$NO + O^{2-} \rightarrow NO_2 \quad (2)$$

where "□" represents an empty position originating from the removal of O^{2-} from the lattice.[52] The ratio of Ce^{3+}/Ce for the samples could be calculated from the results of XPS analysis, and the results are listed in Table 2. Obviously, the Ce^{3+}/Ce ratio of the CeCrLa/TiO_2 catalyst is higher than that of the CeCrM/TiO_2 (M = Cu, Fe) catalyst, which indicates that the introduction of La promotes the conversion of Ce^{4+} to Ce^{3+}. However, the doping of bimetallic oxides led to the increase of Ce^{3+}/Ce ratio in CeCrLaCu/TiO_2 and CeCrLaFe/TiO_2 catalysts, indicating that the synergistic effect of LaCu or LaFe played an important role in the formation of Ce^{3+}.

The XPS spectra for Cr 2p of all samples are given in Figure 5D and show that two distinct peaks correspond to Cr^{3+} (577.6−578.8 eV) and Cr^{6+} (579.8−581.0 eV).[14,15] It has been reported that the addition of Cr could facilitate the SCR performance by the valence change between Cr^{6+} and lower oxidized states (Cr^{5+}, Cr^{3+}, and Cr^{2+}).[16,53] It is obvious that most Cr species in catalysts exist in the form of Cr^{6+}. It is noteworthy that the Cr^{6+}/Cr ratio (Table 2) of CuCrLaCu/TiO_2 (68%) is higher than those of CeCrCu/TiO_2 (54%) and CeCrLa/TiO_2 (61%). The Cr^{6+}/Cr ratio of CeCrLaFe/TiO_2 (63%) was similar to those of CeCrLa/TiO_2 (61%) and CeCrFe/TiO_2 (63%), indicating that the doping of LaCu was conducive to the formation of Cr^{6+} and the synergistic effect of LaCu was stronger than that of LaFe.

The XPS spectra of Cu 2p of the catalysts are shown in Figure 5E. Both peaks of 932.2 eV and 952.1 eV ought to be attributed to Cu^+ species, and the peaks at 953.1 eV and 933.1 eV should be ascribed to Cu^{2+}.[54] As shown in Table 2, the ratio of Cu^+/Cu on the surface of the CeCrLaCu/TiO_2 catalyst is slightly higher than that of the CeCrCu/TiO_2 catalyst. The doping of La leads to the increase of the Cu^+/Cu ratio on the surface, indicating that the synergistic effect of LaCu contributes to the formation of surface Cu^+.

The Fe element was present in the catalyst mainly in two valence states, Fe^{2+} and Fe^{3+}, and was attributed to BE = 702.9 eV, 716.1 eV and BE = 711.6 eV, 733.8 eV, respectively, in Figure 5F. The content of Fe^{2+} and Fe^{3+} in the catalysts was closely related to the formation of oxygen vacancies in the catalyst. From reactions (3, 4), it is known that Fe^{2+} and Fe^{3+} produce O^{2-} during the mutual conversion process. The effect is the same as that of Ce^{3+}. Therefore, the greater the Fe^{2+} content, the more the oxygen adsorption site, and the better the denitration activity of the catalyst.

$$Fe^{2+} + O_2 + \square \rightarrow Fe^{3+} + O^{2-} \quad (3)$$

https://doi.org/10.1021/acsomega.2c04603
ACS Omega 2022, 7, 37694−37704

$$NO + O^{2-} \rightarrow NO_2 \quad (4)$$

The relative contents of Fe^{2+}/Fe were calculated and are listed in Table 2. Compared with the $CeCrFe/TiO_2$ catalyst, the $CeCrLaFe/TiO_2$ catalyst has lower Fe^{2+}, but its catalytic performance is better than the $CeCrFe/TiO_2$ catalyst. Due to the lower ionization energy of $La^{2+} \rightarrow La^{3+}$, electrons are easy to be lost and may be more easily transferred from La to the active component.[55] The incorporation of La facilitates the transformation from low-valence species (Fe^{2+}) to the stable high-valence species (Fe^{3+}).[56]

Figure 5G shows the La 3d spectra. Both La $3d_{3/2}$ and La $3d_{5/2}$ have double peaks, which meant that companion peaks appear. Due to the ionization of electrons in the inner shell layers of La $3d_{3/2}$ and La $3d_{5/2}$, the transfer of 2p valence electrons from the La-coordinated oxygen to the 4f vacant orbital of La results in the splitting of the La 3d characteristic peak and the resultant vibrational companion peaks of La $3d_{3/2}$ and La $3d_{5/2}$. So, the change in the intensity of the companion peak can reflect the ability of the 2p electrons of oxygen to give La.[57] Compared with $CeCrLa/TiO_2$ catalysts, $CeCrLaFe/TiO_2$ and $CeCrLaCu/TiO_2$ catalysts have stronger companion peak intensities, indicating that Fe/Cu promotes the electron supply of O 2p. The electron transfer on the catalyst surface is of great significance for NH_3-SCR. From the XPS analysis in this paper, it is known that the incorporation of La promotes the transfer of electrons between the active components. Doping of LaFe/LaCu is by surface charge transfer doping.[58] And the LaCu/LaFe dopant is in surface contact with the TiO_2 carrier, and the former is used to transfer charges to the carrier based on the difference in the ability of the former to gain and lose electrons.

2.2.5. H_2-TPR Analysis. The redox property of the samples was determined by H_2-TPR analysis, and the results are shown in Figure 6. The H_2 consumption values of all samples are shown in Table 2. Five peaks appear from 250 to 750 °C in the H_2-TPR profile of $CeCrCu/TiO_2$. It has been reported that CuO_x species have a great degree of reduction capacity at lower temperatures.[59] Thus, two reduction peaks of CuO_x could be seen at 339 and 422 °C, respectively, which are due to two reduction steps, that of CuO into Cu_2O and Cu_2O into Cu;[60,61] the reduction peak appearing at 483 °C belongs to the reduction of $Cr^{6+} \rightarrow Cr^{3+}$;[62] the peak at 550 °C is attributed to $Ce^{4+} \rightarrow Ce^{3+}$;[31] and the peak at 631 °C is attributed to crystal lattice CeO_2/Ce_2O_3 and $Cr^{3+} \rightarrow Cr$.[62,6362,63] For the $CeCrFe/TiO_2$ catalyst, the reduction peaks appearing at 570 °C belong to the reduction of $Cr^{6+} \rightarrow Cr^{3+}$ and $Fe_2O_3 \rightarrow Fe_3O_4$.[64] The reduction peak at 630 °C belongs to the reduction of $FeO \rightarrow Fe^0$ and the transformations of surface CeO_2/Ce_2O_3.[65] The H_2 reduction peaks at 695 °C may be due to overlapping of transformations of surface CeO_2/Ce_2O_3 and $Cr^{3+} \rightarrow Cr$.[66] The reduction peaks at 763 °C were attributed to lattice oxygen contained in bulk CeO_2.[62] As for $CeCrLa/TiO_2$, the reduction peak can be divided into four peaks. The reduction peaks appearing at 565 °C belong to the reduction of $Cr^{6+} \rightarrow Cr^{3+}$;[67] the peaks at 617 and 707 °C are respectively attributed to transformations of surface CeO_2/Ce_2O_3 and crystal lattice CeO_2/Ce_2O_3;[68] and the peak at 664 °C might be assigned to $Cr^{3+} \rightarrow Cr$.[69] After the introduction of La, the peak positions move to a higher temperature and the peak area gradually decreases, indicating that the reducibility of the $CeCrLa/TiO_2$ catalyst decreases.

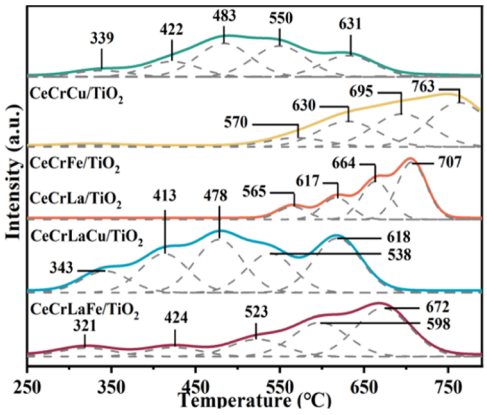

Figure 6. H_2-TPR profiles of the catalysts.

The reduction profiles of the $CeCrLaCu/TiO_2$ catalyst are composed of five main hydrogen consumption steps. Compared with the $CeCrCu/TiO_2$ catalyst, the reduction peak position of the $CeCrLaCu/TiO_2$ catalyst is basically unchanged. And compared with the $CeCrLa/TiO_2$ catalyst, the reduction peak position of the $CeCrLaCu/TiO_2$ catalyst shifted to a lower temperature, such as the reduction temperature of $Ce^{4+} \rightarrow Ce^{3+}$ and $Cr^{6+} \rightarrow Cr^{3+}$ decreases. This indicates that Ce and Cr become more reducible, which can be attributed to the synergistic effect of LaCu. At the same time, the introduction of La increases the hydrogen consumption of Cu and Cr, indicating that the synergistic effect of LaCu is more conducive to improving the redox performance of the catalyst. Similarly, compared with $CeCrLa/TiO_2$ and $CeCrFe/TiO_2$ catalysts, the reduction peak position of $CeCrLaFe/TiO_2$ catalysts shifted to lower temperatures, and the introduction of La increases the reduction peak area of Fe (321 and 424 °C) and Cr (523 and 672 °C), indicating that the synergistic effect between LaFe is beneficial to improve redox performance of catalysts, which is consistent with the result of the improved low-temperature activity of $CeCrLaFe/TiO_2$.

2.2.6. NH_3-TPD Analysis. NH_3-TPD tests were performed, and the results are shown in Figure 7. The total NH_3 adsorption capacity is summarized in Table 3. From Figure 7, three peaks appear from 100 to 500 °C in the NH_3-TPD profile of each catalyst. The peaks at the range of 150−250, 250−400, and 400−550 °C refer to weak acid, medium-strength acid, and high-strength acid, respectively.[70,71] According to the literature,[72] the medium-strength and high-strength acid sites are effective for NO reduction at moderate to high temperature. The NH_3

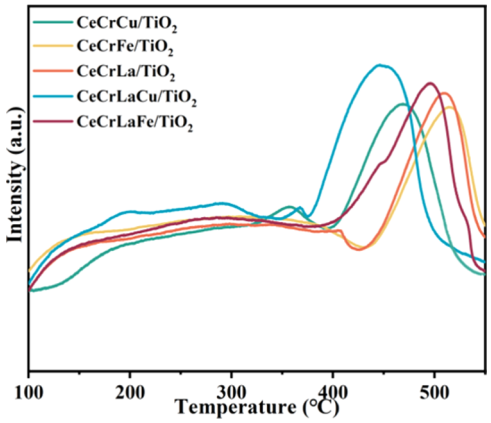

Figure 7. NH_3-TPD profiles of all samples.

https://doi.org/10.1021/acsomega.2c04603
ACS Omega 2022, 7, 37694−37704

Table 3. NH_3 Adsorption Capacity of the Catalysts

samples	total NH_3 uptake (mmol/g)	acidity (mmol/g)		
		weak	moderate	strong
$CeCrCu/TiO_2$	0.130	0.038	0.032	0.060
$CeCrFe/TiO_2$	0.132	0.035	0.041	0.056
$CeCrLa/TiO_2$	0.133	0.051	0.020	0.062
$CeCrLaCu/TiO_2$	0.173	0.045	0.050	0.078
$CeCrLaFe/TiO_2$	0.164	0.041	0.060	0.063

uptake of these catalysts in descending order is $CeCrLaCu/TiO_2$ > $CeCrLaFe/TiO_2$ > $CeCrLa/TiO_2$ > $CeCrFe/TiO_2$ > $CeCrCu/TiO_2$. The NH_3 adsorption capacity of the catalyst is proportional to the catalytic performance, indicating that the NH_3 adsorption capacity plays an important role in the catalytic system.[73,74] Compared with $CeCrLa/TiO_2$ and $CeCrCu/TiO_2$ catalysts, the NH_3 adsorption capacity of $CeCrLaCu/TiO_2$ and $CeCrLaFe/TiO_2$ catalysts was significantly improved, indicating that the synergistic effect of LaCu/LaFe promoted the surface acidity of the catalysts, which could provide more ad-NH_3 species for the NH_3-SCR reaction. Compared with the $CeCrLaFe/TiO_2$ catalyst, the $CeCrLaCu/TiO_2$ catalyst has stronger NH_3 adsorption capacity, so it is more conducive to NH_3-SCR performance.

3. CATALYTIC HYDROTHERMAL AGING

As shown in Figure 8, when the temperature is less than 300 °C, the activities of all catalysts have a sharp decrease; this may be due to the reduction of catalyst active sites due to hydrothermal aging.[75] It can be concluded that hydrothermal aging has a great influence on low temperature catalysis. $CeCrLaCu/TiO_2$-H and $CeCrLaFe/TiO_2$-H still maintain good activity while the temperature is greater than 300 °C, and the NO conversion drops from 99.5 to 95%, which shows that the synergistic effect of LaCu and LaFe is better for hydrothermal stability. In general, hydrothermal aging has an acceptable effect on catalysts in this article (Figure 8).

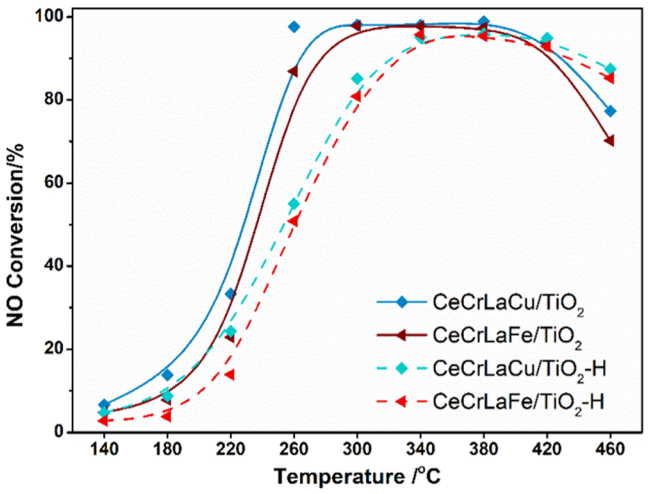

Figure 8. NO conversion of catalysts after hydrothermal aging. Reaction conditions: [NO] = [NH_3] = 1000 ppm, [O_2] = 5%, N_2 balance, GHSV = 20,000 h^{-1}.

4. CONCLUSIONS

In this paper, a series of $CeCrM/TiO_2$ (M = Cu, Fe, La, LaCu, LaFe) catalysts were prepared. By mixing low-dose components, a good low-temperature denitrification catalyst $CeCrLaCu/TiO_2$ was selected. The catalyst has excellent NH_3-SCR performance in a wide temperature window. XRD analysis showed that the synergistic effect of LaCu and LaFe could effectively reduce the aggregation of active species and promote the high dispersion of active components on the surface of TiO_2. The addition of LaCu and LaFe changed the redox state and surface species concentration of the catalysts. The synergistic effect of LaCu/LaFe promoted the formation of Ce^{3+} and Cr^{6+}, and the synergistic effect of LaCu was stronger. The $CeCrLaCu/TiO_2$ catalyst has the highest relative atomic ratio (Ce^{3+}/Ce^{n+}, Cr^{6+}/Cr, Cu^{+}/Cu, and O_α/O_β). It is beneficial for redox of reactive gas on the catalyst surface. The results of H_2-TPR and NH_3-TPD showed that the synergistic effect of LaCu improved the redox capacity and surface acidity of the catalyst, which was an important reason for the excellent performance of the NH_3-SCR catalyst.

5. EXPERIMENTAL SECTION

5.1. Catalyst Preparation. *5.1.1. Preparation of Supports.* A certain amount of metatitanic acid ($TiO(OH)_2$, Xiya Reagent, China, 98%) was calcined at 500 °C for 3 h in air.

5.1.2. Preparation of Catalysts. The catalyst was prepared by the impregnation method. TiO_2 powder and specific amounts of $Ce(NO_3)_3{\cdot}6H_2O$, $Cr(NO_3)_3{\cdot}9H_2O$, $La(NO_3)_3{\cdot}6H_2O$, $Cu(NO_3)_2{\cdot}6H_2O$, and $Fe(NO_3)_3{\cdot}9H_2O$ were mixed together in absolute ethanol, and the mixture was stirred in a magnetic stirrer at room temperature for 6 h. The mixture was aged at room temperature for 24 h and then dried at 80 °C for 12 h, followed by calcination at 450 °C for 4 h in a muffle furnace. CeO_x, CrO_x, LaO_x, and CuO_x (FeO_x) mixed metal oxides are obtained after calcination. The solid sample was crushed and sieved to 40−60 mesh and was recorded as $CeCrM_x/TiO_2$ (M = La, Cu, Fe, LaCu, LaFe). The active ingredient ratio of catalysts Ce/Cr/La/Fe/Cu was 4:3:2:8:8.

5.1.3. Preparation of Hydrothermal Aging Catalysts. The hydrothermal aging conditions are as follows: 5% CO_2, 5% H_2O, 5% O_2, and N_2 as equilibrium gases, 700 °C for 12 h.

5.2. Catalyst Characterization. *5.2.1. X-ray Diffraction (XRD).* An X-ray diffractometer (Rigaku Ultima IV) was used in determining the catalyst crystal structures using these parameters: scanning at 2θ range from 10 to 80° and radiation at 40 mA and 40 kV with Cu Kα (λ = 0.15406 nm).

5.2.2. Brunauer−Emmett−Teller (BET) Surface Area Analysis. A Micromeritics ASAP 2460 was used to perform the test of N_2 adsorption−desorption for the measurement of the textural characteristics of the catalysts at a liquid nitrogen temperature of −196 °C. To remove physically adsorbed species, the catalysts were pre-degassed for 10 h at 200 °C before each analysis. The pore size distribution and specific surface area of the catalysts were calculated using the Barrett−Joyner−Halenda (BJH) method and the Brunauer−Emmet−Teller (BET) equation.

5.2.3. Scanning Electron Microscopy (SEM). An FEI Apreo was used to examine the morphology of the catalysts. The sample was dispersed on the conductive adhesive and then sprayed gold to observe.

5.2.4. X-Ray Photoelectron Spectroscopy (XPS). An Escalab 250Xi with a monochromatic Al-Kα target ($h\upsilon$ = 1486.6 eV) was used to obtain X-ray photoelectron spectroscopy (XPS) of the

https://doi.org/10.1021/acsomega.2c04603
ACS Omega 2022, 7, 37694−37704

samples. Before the test, the samples were outgassed in a UHV chamber ($<10^{-7}$ Pa). The calibration of binding energies of O 1s, Ti 2p, Ce 3d, Cr 2p, Cu 2p, and Fe 2p was obtained using the C 1s peak (284.8 eV). Peak fitting is done using XPSPEAK 4.1 with a Shirley background.

5.2.5. Temperature-Programmed Reduction by Hydrogen (H_2-TPR). A chemisorption apparatus (Micromeritics ChemiSorb 2720) with 0.2 g of catalyst was used to collect H_2-TPR profiles. Before that, the samples were pretreated in a pure Ar atmosphere for 1 h at 300 °C and then cooled to 50 °C for half an hour to mix the gas 10% H_2/Ar. The TPR profiles of the catalysts were collected when the baseline remained unchanged by heating the samples from 50 to 800 °C at a rate of 10 °C/min, with an aggregation rate of 25 mL/min with 10% H_2/Ar. Thermal conductivity detectors were taken in continuously monitoring H_2 consumption.

5.2.6. Temperature-Programmed Desorption by Ammonia (NH_3-TPD). A chemisorption apparatus (Micromeritics Auto Chem II 2920) with 0.2 g of catalyst was used to collect NH_3-TPD profiles. Before that, the catalysts were preheated for 1 h at 300 °C in a helium flow and then cooled to 100 °C for 5% NH_3/He 1 h. The physically adsorbed NH_3 was removed by purging He for another 1 h. When the samples were heated at a rate of 10 °C/min from 100 to 500 °C, with an aggregation rate of 50 mL/min with He, the profiles of the catalysts were recorded.

5.3. Catalytic Performance Measurement. In this work, a fixed-bed flow reactor containing 3 mL of catalyst of 40−60 mesh was taken for testing SCR activities. The reaction condition was controlled as follows: 1000 ppm NO, 1000 ppm NH_3, 5% O_2, and the balance gas is N_2. The gas hourly space velocity (GHSV) was approximately 20,000 h^{-1} with a sum rate of 1000 mL/min of the feed gas. The NO concentration was measured with a signal NO_x analyzer (KM945, KANE, U.K.). The following equation was used to calculate NO conversion

$$\text{NO conversion}(\%) = \frac{[\text{NO}]_{\text{in}} - [\text{NO}]_{\text{out}}}{[\text{NO}]_{\text{in}}} \times 100\% \quad (5)$$

AUTHOR INFORMATION

Corresponding Authors

Shanshan Liu − *College of Chemical and Biological Engineering, Shandong University of Science and Technology, Qingdao 266590, P. R. China*; Email: skd996368@sdust.edu.cn

Xintang Zhang − *College of Chemical and Biological Engineering, Shandong University of Science and Technology, Qingdao 266590, P. R. China*; Email: zhangxt966@126.com

Authors

Guilin Mu − *College of Chemical and Biological Engineering, Shandong University of Science and Technology, Qingdao 266590, P. R. China*; orcid.org/0000-0003-2525-6259

Shuai Liu − *College of Chemical and Biological Engineering, Shandong University of Science and Technology, Qingdao 266590, P. R. China*

Qingjie Liu − *College of Chemical and Biological Engineering, Shandong University of Science and Technology, Qingdao 266590, P. R. China*

Complete contact information is available at: https://pubs.acs.org/10.1021/acsomega.2c04603

Notes

The authors declare no competing financial interest.

No conflict of interest exits in the submission, and the manuscript is approved by all authors for publication. I would like to declare on behalf of my co-authors that the work described was original research that has not been published previously in whole or in part.

ACKNOWLEDGMENTS

The authors thank Prof. Zhang and Dr. Liu for their help in designing the experiment and writing the paper and also thank S.L. and Q.L. for their help in the process of the experiment. This research did not receive any specific grant from funding agencies in the public, commercial, or not-for-profit sectors.

REFERENCES

(1) Ren, S.; Guo, F. Q.; Yang, J.; Yao, L.; Zhao, Q.; Kong, M. Selection of carbon materials and modification methods in low-temperature sintering flue gas denitrification. *Chem. Eng. Res. Des.* **2017**, *126*, 278−285.

(2) Chu, S.; Zhou, W.; Zhang, C.; Zheng, Y.; Liu, Y.; Liu, Y. Relationship between the structure and catalytic performance of MoS_2 with different surfactant-assisted syntheses in the hydrodesulfurization reaction of 4,6-DMDBT. *RSC Adv.* **2020**, *10*, 7600−7608.

(3) Tong, J. B.; Lin, Y.; Liu, S. L.; Wen, J. T.; Liu, Y. Y. Recent progress in the support of hydrodesulfurization catalysts. *Chem. Ind. Eng. Prog.* **2014**, *33*, 1170−1179.

(4) Liu, X. Y.; Zhang, P.; Jia, Y. Y.; Tang, Z. H.; Liu, G. L.; Wu, S. F. Research progresses of TiO_2 supported manganese-ceriumcatalyst for low-temperature SCR denitration. *Environ. Prot. Chem. Ind.* **2020**, *40*, 26−31.

(5) Ganjkhanlou, Y.; Janssens, T. V. W.; Vennestrøm, P. N. R.; Mino, L.; Paganini, M. C.; Signorile, M.; Bordiga, S.; Berlier, G. Location and activity of VO_x species on TiO_2 particles for NH_3-SCR catalysis. *Appl. Catal., B* **2020**, *278*, No. 119337.

(6) Thirupathi, B.; Smirniotis, P. G. Co-doping a metal (Cr, Fe, Co, Ni, Cu, Zn, Ce, and Zr) on Mn/TiO_2 catalyst and its effect on the selective reduction of NO with NH_3 at low-temperatures. *Appl. Catal., B* **2011**, *110*, 195−206.

(7) Saeidi, M.; Hamidzadeh, M. Co-doping a metal (Cr, Mn, Fe, Co, Ni, Cu, and Zn) on Mn/ZSM-5 catalyst and its effect on the catalytic reduction of nitrogen oxides with ammonia. *Res. Chem. Intermed.* **2017**, *43*, 2143−2157.

(8) Guo, L. L.; Liu, L.; Zhu, X. L.; Zhang, Q.; Li, C. Y. Effect of Mg/Al molar ratios on NO reduction activity of CO using Ce-La/$MgAl_2O_{4-x}$ catalysts. *J. Fuel Chem. Technol.* **2017**, *45*, 723−730.

(9) Hou, X. X.; Chen, H. P.; Liang, Y. H.; Wei, Y. L.; Li, Z. Q. La Modified Fe-Mn/TiO_2 Catalysts to Improve SO_2 Resistance for NH_3-SCR at Low-Temperature. *Catal. Surv. Asia* **2020**, *24*, 291−299.

(10) Liu, C.; Chen, L.; Li, J.; Ma, L.; Arandiyan, H.; Du, Y.; Xu, J.; Hao, J. Enhancement of activity and sulfur resistance of CeO_2 supported on TiO_2-SiO_2 for the selective catalytic reduction of NO by NH_3. *Environ. Sci. Technol.* **2012**, *46*, 6182−6189.

(11) Gao, R. H.; Zhang, D. S.; Maitarad, P.; Shi, L. Y.; Rungrotmongkol, T.; Li, H. R.; Zhang, J. P.; Cao, W. G. Morphology-Dependent Properties of MnO_x/ZrO_2−CeO_2 Nanostructures for the Selective Catalytic Reduction of NO with NH_3. *J. Phys. Chem. C* **2013**, *117*, 10502−10511.

(12) Sun, P.; Guo, R. T.; Liu, S. M.; Wang, S. X.; Pan, W. G.; Li, M. Y.; Liu, S. W.; Liu, J.; Sun, X. Enhancement of the low-temperature activity of Ce/TiO_2 catalyst by Sm modification for selective catalytic reduction of NO_x with NH_3. *Mol. Catal.* **2017**, *433*, 224−234.

(13) Chen, L.; Li, J. H.; Ge, M. F.; Ma, L.; Chang, H. Z. Mechanism of Selective Catalytic Reduction of NO_x with NH_3 over CeO_2-WO_3 Catalysts. *Chin. J. Catal.* **2011**, *32*, 836−841.

(14) Su, J.; Yao, W. Y.; Liu, Y.; Wu, Z. B. The impact of CrO_x loading on reaction behaviors of dichloromethane (DCM) catalytic combustion over Cr-O/HZSM-5 catalysts. *Appl. Surf. Sci.* **2017**, *396*, 1026−1033.

(15) Wang, Z. Y.; Guo, R. T.; Guan, Z. Z.; Shi, X.; Pan, W. G.; Fu, Z. G.; Qin, H.; Liu, X. Y. The promotion effect of Cr additive on $CeZr_2O_x$ catalyst for the low-temperature selective catalytic reduction of NO_x with NH_3. *Appl. Surf. Sci.* **2019**, *485*, 133−140.
(16) Cai, W.; Zhong, Q.; Zhang, S. L.; Zhang, J. X. Effects of Cr on the NO oxidation over the ceria−zirconia solid solution. *RSC Adv.* **2013**, *3*, 7009−7015.
(17) Cai, W.; Zhong, Q.; Yu, Y.; Dai, S. Correlation of morphology with catalytic performance of $CrO/Ce_{0.2}Zr_{0.8}O_2$ catalysts for NO oxidation via in-situ STEM. *Chem. Eng. J.* **2016**, *288*, 238−245.
(18) Lu, M.; Hou, H. L.; Wei, C. Y.; Guan, X. H.; Wei, W.; Wang, G. S. Preparation of Quasi-MIL-101(Cr) Loaded Ceria Catalysts for the Selective Catalytic Reduction of NO_x at Low Temperature. *Catalysts* **2020**, *10*, 140.
(19) Chen, D.; Cen, C.; Feng, J.; Yao, C.; Xiong, Y.; et al. Co-catalytic effect of Al-Cr pillared montmorillonite as a new SCR catalytic support. *J. Chem. Technol. Biotechnol.* **2016**, *91*, 2842−2851.
(20) Gao, E.; Huang, B.; Zhao, Z.; Pan, H.; Zhang, W.; Li, Y.; Bernards, M. T.; He, Y.; Shi, Y. Understanding the co-effects of manganese and cobalt on the enhanced SCR performance for $Mn_xCo_{1-x}Cr_2O_4$ spinel-type catalysts. *Catal. Sci. Technol.* **2020**, *10*, 4752−4765.
(21) Li, F.; Xie, J.; Qi, K.; Gong, P.; He, F. Evaluating the Intermetallic Interaction of Fe or Cu Doped Mn/TiO_2 Catalysts: SCR Activity and Sulfur Tolerance. *Catal. Lett.* **2019**, *149*, 788−797.
(22) Jiang, L. J.; Liu, Q. C.; Zhao, Q.; Ren, S.; Kong, M.; Yao, L.; Meng, F. Promotional effect of Ce on the SCR of NO with NH_3 at low temperature over MnO_x supported by nitric acid-modified activated carbon. *Res. Chem. Intermed.* **2018**, *44*, 1729−1744.
(23) Bin, F.; Wei, X. L.; Li, B.; Hui, K. S. Self-sustained combustion of carbon monoxide promoted by the Cu-Ce/ZSM-5 catalyst in $CO/O_2/N_2$ atmosphere. *Appl. Catal., B* **2015**, *162*, 282−288.
(24) Gao, Q.; Han, S.; Ye, Q.; Cheng, S. Y.; Kang, T. F.; Dai, H. X. Effects of Lanthanide Doping on the Catalytic Activity and Hydrothermal Stability of Cu-SAPO-18 for the Catalytic Removal of NO_x (NH_3-SCR) from Diesel Engines. *Catalysts* **2020**, *10*, 336.
(25) Lu, P.; Li, C. T.; Zeng, G. M.; He, L. J.; Peng, D. L.; Cui, H. F.; Li, S. H.; Zhai, Y. B. Low temperature selective catalytic reduction of NO by activated carbon fiber loading lanthanum oxide and ceria. *Appl. Catal., B* **2010**, *96*, 157−161.
(26) Yi, H. H.; Yang, K.; Tang, X. L.; Zhao, S. Z.; Gao, F. Y.; Huang, Y. H.; Shi, Y. R.; Xie, X. Z.; Zhang, R. C. Promoting Simultaneous Desulfurization and Denitrification Performance of Al_2O_3@TiO_2 Core−Shell Structure Adsorbents by Enhancing Oxidation Performance: Modification by Rare Earth Elements (La, Ce, and Y), Reaction Temperature, and Oxygen Concentration. *Ind. Eng. Chem. Res.* **2019**, *58*, 5423−5431.
(27) Zhang, D. J.; Ma, Z. R.; Wang, B. D.; Sun, Q.; Xu, W. Q.; Zhu, T. Effects of MO (M=Mn, Cu, Sb, La) on V−Mo−Ce/Ti selective catalytic reduction catalysts. *J Rare Earth* **2020**, *38*, 157−166.
(28) Guo, R.-t.; Zhen, W.; Pan, W.; Zhou, Y.; Hong, J.; et al. Effect of Cu doping on the SCR activity of CeO_2 catalyst prepared by citric acid method. *J. Ind. Eng. Chem.* **2014**, *20*, 1577−1580.
(29) Guan, B.; Jiang, H.; Peng, X.; Wei, Y.; Liu, Z.; Chen, T.; Lin, H.; Huang, Z. Promotional effect and mechanism of the modification of Ce on the enhanced NH_3-SCR efficiency and the low temperature hydrothermal stability over Cu/SAPO-34 catalysts. *Appl. Catal., A* **2021**, *617*, No. 118110.
(30) Schill, L.; Putluru, S. S. R.; Schill, L.; Jensen, A. D. Effect of Fe doping on low temperature deNO_x activity of high-performance vanadia anatase nanoparticles. *Catal. Commun.* **2014**, *56*, 110−114.
(31) Zhang, K.; Wang, J.; Guan, P.; Li, N.; Gong, Z.; Zhao, R.; Luo, H.; Wu, W. Low-temperature NH_3-SCR catalytic characteristic of Ce-Fe solid solutions based on rare earth concentrate. *Mater. Res. Bull.* **2020**, *128*, No. 110871.
(32) Ge, T. T.; Zhu, B. Z.; Sun, Y. L.; Song, W. Y.; Fang, Q. L.; Zhong, Y. X. Investigation of low-temperature selective catalytic reduction of NO_x with ammonia over Cr-promoted Fe/AC catalysts. *Environ. Sci. Pollut. Res. Int.* **2019**, *26*, 33067−33075.
(33) Pan, S. W.; Luo, H. C.; Li, L.; Wei, Z. L.; Huang, B. C. H_2O and SO_2 deactivation mechanism of MnO_x/MWCNTs for low-temperature SCR of NO_x with NH_3. *J. Mol. Catal. A* **2013**, *377*, 154−161.
(34) Chen, L.; Ren, S.; Xing, X. D.; Yang, J.; Yang, J.; Wang, M. M.; Chen, Z. C.; Liu, Q. C. Low-Cost CuX Catalyst from Blast Furnace Slag Waste for Low-Temperature NH_3-SCR: Nature of Cu Active Sites and Influence of SO_2/H_2O. *ACS Sustainable Chem. Eng.* **2022**, *10*, 7739−7751.
(35) Hao, S. J.; Cai, Y. D.; Sun, C. Z.; Sun, J. F.; Tang, C. J.; Dong, L. High Resistance of SO_2 and H_2O over Monolithic Mn-Fe-Ce-Al-O Catalyst for Low Temperature NH_3-SCR. *Catalysts* **2020**, *10*, 1329.
(36) Zhang, Y. N.; Zhu, H. C.; Zhang, T.; Li, J. J.; Chen, J. J.; Peng, Y.; Li, J. H. Revealing the Synergistic Deactivation Mechanism of Hydrothermal Aging and SO_2 Poisoning on Cu/SSZ-13 under SCR Condition. *Environ. Sci. Technol.* **2022**, *56*, 1917−1926.
(37) Xie, S. Z.; Li, L. L.; Jin, L. J.; Wu, Y. H.; Liu, H.; Qin, Q. J.; Wei, X. L.; Liu, J. X.; Dong, L. H.; Li, B. Low temperature high activity of M (M = Ce, Fe, Co, Ni) doped M-Mn/TiO_2 catalysts for NH_3-SCR and in situ DRIFTS for investigating the reaction mechanism. *Appl. Surf. Sci.* **2020**, *515*, No. 146014.
(38) Ren, J.; Ren, M. J.; Wang, D. L.; Lin, J. Y.; Li, Z. Mechanism of microwave-induced carbothermic reduction and catalytic performance of Cu/activated carbon catalysts in the oxidative carbonylation of methanol. *J. Therm. Anal. Calorim.* **2015**, *120*, 1929−1939.
(39) Han, F.; Xu, C.; Sun, W. Z.; Yu, S. T.; Xian, M. Effective removal of salicylic and gallic acids from single component and impurity-containing systems using an isatin-modified adsorption resin (vol 7, pg 23164, 2017). *RSC Adv.* **2017**, *7*, 26370.
(40) Wang, S. H.; Fan, C.; Zhao, Z. Q.; Liu, Q.; Xu, G.; Wu, M. H.; Chen, J. J.; Li, J. H. A facile and controllable in situ sulfation strategy for CuCeZr catalyst for NH_3-SCR. *Appl. Catal., A* **2020**, *597*, No. 117554.
(41) Gao, E. H.; Su, G. J.; Zhang, W.; Bernards, M. T.; He, Y.; Pan, H.; Shi, Y. Surface lattice oxygen activation via Zr^{4+} cations substituting on $A^{(2+)}$ sites of $MnCr_2O_4$ forming $Zr_xMn_{1-x}Cr_2O_4$ catalysts for enhanced NH_3-SCR performance. *Chem. Eng. J.* **2020**, *380*, No. 122397.
(42) Li, S. H.; Huang, B. C.; Yu, C. L. A CeO_2-MnO_x core-shell catalyst for low-temperature NH_3-SCR of NO. *Catal. Commun.* **2017**, *98*, 47−51.
(43) Yao, X. J.; Ma, K. L.; Zou, W. X.; He, S. G.; An, J. B.; Yang, F. M.; Dong, L. Influence of preparation methods on the physicochemical properties and catalytic performance of MnO_x-CeO_2 catalysts for NH_3-SCR at low temperature. *Chin. J. Catal.* **2017**, *38*, 146−159.
(44) Yao, X. J.; Kong, T. T.; Yu, S. H.; Li, L. L.; Yang, F. M.; Dong, L. Influence of different supports on the physicochemical properties and denitration performance of the supported Mn-based catalysts for NH_3-SCR at low temperature. *Appl. Surf. Sci.* **2017**, *402*, 208−217.
(45) Peng, Y.; Li, K. Z.; Li, J. H. Identification of the active sites on CeO_2−WO_3 catalysts for SCR of NO_x with NH_3: An in situ IR and Raman spectroscopy study. *Appl. Catal., B* **2013**, *140-141*, 483−492.
(46) Yang, J.; Li, Z. F.; Yang, C. L.; Ma, Y. Y.; Li, Y. Y.; Zhang, Q.; Song, K.; Cui, J. X. Significant promoting effect of La doping on the wide temperature NH_3-SCR performance of Ce and Cu modified ZSM-5 catalysts. *J. Solid State Chem.* **2022**, *305*, No. 122700.
(47) Lee, K. J.; Kumar, P. A.; Maqbool, M. S.; Rao, K. N.; Song, K. H.; Ha, H. P. Ceria added Sb-V_2O_5/TiO_2 catalysts for low temperature NH_3 SCR: Physico-chemical properties and catalytic activity. *Appl. Catal. B.* **2013**, *142−143*, 705−717.
(48) Liu, S. S.; Wang, H.; Wei, Y.; Zhang, R. D. Core-shell structure effect on CeO_2 and TiO_2 supported WO_3 for the NH_3-SCR process. *Mol. Catal.* **2020**, *485*, No. 110822.
(49) Xu, Q.; Su, R. G.; Cao, L.; Li, Y. Q.; Yang, C. Y.; Luo, Y.; Street, J.; Jiao, P. C.; Cai, L. L. Facile preparation of high-performance Fe-doped Ce-Mn/TiO_2 catalysts for the low-temperature selective catalytic reduction of NO_x with NH_3. *RSC Adv.* **2017**, *7*, 48785−48792.
(50) Cheng, J.; Song, L. Y.; Wu, R.; Li, S. N.; Sun, Y. M.; Zhu, H. T.; Qiu, W. G.; He, H. Promoting effect of microwave irradiation on CeO_2-TiO_2 catalyst for selective catalytic reduction of NO by NH_3. *J. Rare Earth* **2020**, *38*, 59−69.

https://doi.org/10.1021/acsomega.2c04603
ACS Omega 2022, 7, 37694−37704

(51) Wang, Q. L.; Zhou, J. J.; Zhang, J. C.; Zhu, H.; Feng, Y. H.; Jin, J. Effect of Ceria Doping on the Catalytic Activity and SO_2 Resistance of MnO_x/TiO_2 Catalysts for the Selective Catalytic Reduction of NO with NH_3 at Low Temperatures. *Aerosol Air Qual. Res.* **2020**, *20*, 477−488.
(52) Wang, R. H.; Hao, Z. F.; Li, Y.; Liu, G. Q.; Zhang, H.; Wang, H. T.; Xia, Y. G.; Zhan, S. H. Relationship between structure and performance of a novel highly dispersed MnO_x on Co-Al layered double oxide for low temperature NH_3-SCR. *Appl. Catal., B* **2019**, *258*, No. 117983.
(53) Yu, Q.; Manfred, R.; Li, L. D.; Kong, F. X.; Wu, G. J.; Guan, N. J. The promotional effect of Cr on catalytic activity of Pt/ZSM-35 for H_2-SCR in excess oxygen. *Catal. Commun.* **2010**, *11*, 955−959.
(54) Wang, X.; Su, J.; et al. Promotional synergistic effect of Cu and Nb doping on a novel Cu/Ti-Nb ternary oxide catalyst for the selective catalytic reduction of NO_x with NH_3. *Appl. Catal., B* **2018**, *220*, 234−250.
(55) Hou, X.; Chen, H.; Liang, Y.; Wei, Y.; Li, Z. La Modified Fe-Mn/TiO_2 Catalysts to Improve SO_2 Resistance for NH_3-SCR at Low-Temperature. *Catal. Surv. Asia* **2020**, *24*, 291−299.
(56) Liu, T. K.; Wei, L. Q.; Yao, Y. Y.; Dong, L. H.; Li, B. La promoted CuO-MnO_x catalysts for optimizing SCR performance of NO with CO. *Appl. Surf. Sci.* **2021**, *546*, No. 148971.
(57) Li, N.; Chen, Z. D.; Bai, X. R.; Hou, L. M.; Jiao, K. L.; Wu, W. F. Study on the mechanism of synthetic (Ce,La)CO3F sulfuric acid acidification and NH_3-SCR loaded with Mn and Fe. *RSC Adv.* **2021**, *11*, 19943−19955.
(58) Ma, L. P.; Ren, W. C.; Cheng, H. M. Progress in Surface Charge Transfer Doping of Graphene. *Acta Phys.-Chim. Sin.* **2022**, *38*, No. 2012080.
(59) Ali, S.; Chen, L. Q.; Li, Z. B.; Zhang, T. R.; Li, R.; Bakhtiar, S. H.; Leng, X. S.; Yuan, F. L.; Niu, X. Y.; Zhu, Y. J. Cu_x-$Nb_{1.1-x}$ (x = 0.45, 0.35, 0.25, 0.15) bimetal oxides catalysts for the low temperature selective catalytic reduction of NO with NH_3. *Appl. Catal., B* **2018**, *236*, 25−35.
(60) Putluru, S. S. R.; Mossin, S.; Riisager, A.; F Ehrmann, R. Heteropoly acid promoted Cu and Fe catalysts for the selective catalytic reduction of NO with ammonia. *Catal. Today* **2011**, *176*, 292−297.
(61) Fan, J.; Ning, P.; Wang, Y. C.; Song, Z. X.; Liu, X.; Wang, H. M.; Wang, J.; Wang, L. Y.; Zhang, Q. L. Significant promoting effect of Ce or La on the hydrothermal stability of Cu-SAPO-34 catalyst for NH_3-SCR reaction. *Chem. Eng. J.* **2019**, *369*, 908−919.
(62) Wang, Z. Y.; Guo, R. T.; Guan, Z. Z.; Shi, X.; Pan, W. G.; Fu, Z. G.; Qin, H.; Liu, X. Y. The promotion effect of Cr additive on $CeZr_2O_x$ catalyst for the low-temperature selective catalytic reduction of NO_x with NH_3. *Appl. Surf. Sci.* **2019**, *485*, 133−140.
(63) Liu, H.; Wei, L.; Yue, R.; Chen, Y. CrO_x-CeO_2 binary oxide as a superior catalyst for NO reduction with NH_3 at low temperature in presence of CO. *Catal. Commun.* **2010**, *11*, 829−833.
(64) Yuan, E. H.; Li, M.; Yang, M. H.; Huang, X. S.; Zhang, K.; Han, W. L.; Tang, Z. C.; Liu, Z. W. Encapsulation of ultra-small Cu-Fe into ZSM-5 zeolites for NH_3-SCR with broad reaction-temperature ranges. *Microporous Mesoporous Mater.* **2022**, *331*, No. 111675.
(65) Jiang, L. J.; Liang, Y.; Liu, W. Z.; Wu, H. L.; Aldahri, T.; Carrero, D. S.; Liu, Q. C. Synergistic effect and mechanism of FeO_x and CeO_x co-doping on the superior catalytic performance and SO_2 tolerance of Mn-Fe-Ce/ACN catalyst in low-temperature NH_3-SCR of NO_x. *J. Environ. Chem. Eng.* **2021**, *9*, No. 106360.
(66) Cai, W.; Zhao, Y. X.; Chen, M. D.; Jiang, X. M.; Wang, H.; Ou, M.; Wan, S. P.; Zhong, Q. The formation of 3D spherical Cr-Ce mixed oxides with roughness surface and their enhanced low-temperature NO oxidation. *Chem. Eng. J.* **2018**, *333*, 414−422.
(67) Gao, E. H.; Huang, B.; Zhao, Z. L.; Pan, H.; Zhang, W.; Li, Y. N.; Bernards, M. T.; He, Y.; Shi, Y. Understanding the co-effects of manganese and cobalt on the enhanced SCR performance for $Mn_{(x)}Co_{(1-x)}Cr_{(2)}O_{(4)}$ spinel-type catalysts. *Catal. Sci. Technol.* **2020**, *10*, 4752−4765.
(68) Yang, C. X.; Zhang, K. X.; Zhang, Y. K.; Peng, G. J.; Yang, M.; Wen, J. J.; Xie, Y.; Xia, F. T.; Jia, L. J.; Zhang, Q. L. An environmental and highly active Ce/Fe-Zr-SO_4^{2-} catalyst for selective catalytic reduction of NO with NH_3: The improving effects of CeO_2 and SO_4. *J. Environ. Chem. Eng.* **2021**, *9*, No. 106799.
(69) Jia, Y.; Yang, J. H.; Jiang, J.; Huang, M. Y.; Guo, L. N.; Zhang, C. W.; Yuan, J.; Gu, M. Y. Low temperature SCR de-NO_x performance and mechanism of heteropolyacid VPO-Cr-PEG/TiO_2 catalyst. *Catal. Commun.* **2021**, *153*, No. 106299.
(70) Li, S. C.; Huang, W. J.; Xu, H. M.; Chen, T. J.; Ke, Y.; Qu, Z.; Yan, N. Q. Alkali-induced deactivation mechanism of V_2O_5-WO_3/TiO_2 catalyst during selective catalytic reduction of NO by NH_3 in aluminum hydrate calcining flue gas. *Appl. Catal., B* **2020**, *270*, No. 118872.
(71) Xu, H. D.; Wang, Y.; Cao, Y.; Fang, Z. T.; Lin, T.; Gong, M. C.; Chen, Y. Q. Catalytic performance of acidic zirconium-based composite oxides monolithic catalyst on selective catalytic reduction of NO_x with NH_3. *Chem. Eng. J.* **2014**, *240*, 62−73.
(72) Chitsazi, H.; Wu, R.; Zhang, N. Q.; He, J. D.; Zhang, G. Z.; He, H. Enhancement of Low-Temperature NH_3-SCR Catalytic Activity and H_2O Resistance Ability Over MnO_x/TiO_2 Catalyst by Expanded Graphite. *Catal. Lett.* **2020**, *150*, 2688−2694.
(73) Zhou, X. M.; Huang, X. Y.; Xie, A. J.; Luo, S. P.; Yao, C.; Li, X. Z.; Zuo, S. X. V_2O_5-decorated Mn-Fe/attapulgite catalyst with high SO_2 tolerance for SCR of NO_x with NH_3 at low temperature. *Chem. Eng. J.* **2017**, *326*, 1074−1085.
(74) Wu, X.; Wang, R. N.; Du, Y. L.; Li, X. J.; Meng, H.; Xie, X. M. NOx removal by selective catalytic reduction with ammonia over hydrotalcite-derived NiTi mixed oxide. *New J. Chem.* **2019**, *43*, 2640−2648.
(75) Chen, L.; Wang, D.; Wang, J. D.; Weng, D.; Cao, L. Hydrothermal and sulfur aging of CeTi/CeWTi catalysts for selective catalytic reduction of NO_x with NH_3. *J Rare Earth* **2019**, *37*, 829−836.

https://doi.org/10.1021/acsomega.2c04603
ACS Omega 2022, 7, 37694−37704